Towards the Origin of the Nonlinear Response in Hybrid Plasmonic Systems

Tobias Utikal,[1,2] Thomas Zentgraf,[1] Thomas Paul,[3] Carsten Rockstuhl,[3] Falk Lederer,[3]
Markus Lippitz,[1,2] and Harald Giessen[1]

[1]*4th Physics Institute and Research Center SCoPE, University of Stuttgart, Pfaffenwaldring 57, 70550 Stuttgart, Germany*
[2]*Max Planck Institute for Solid State Research, Heisenbergstraße 1, 70569 Stuttgart, Germany*
[3]*Institute for Condensed Matter Theory and Solid State Optics, Abbe Center of Photonics, Friedrich-Schiller-Universität Jena,
Max-Wien Platz 1, 07743 Jena, Germany*

Plasmonic systems are known for their distinct nonlinear optical properties when compared to purely dielectric materials. Although it is well accepted that the enhanced nonlinear processes in plasmonic-dielectric compounds are related to the excitation of localized plasmon resonances, their exact origin is concealed by the local field enhancement in the surrounding material and the nonlinearity in the metal. Here, we show that the origin of third-harmonic generation in hybrid plasmonic-dielectric compounds can be unambiguously identified from the shape of the nonlinear spectrum.

In nonlinear optics, the linear optical properties of a resonant system usually determine the shape of the non-linear spectrum. In the simplest picture, the anharmonicity term of an oscillator at high light intensities is responsible for the nonlinear response [1]. For example, early investigations showed that enhanced second-harmonic generation at metal surfaces can be related to surface plasmon excitations [2,3].

However, in plasmonic nanostructures [4–9] and meta-materials [10–12] the nonlinear response is not simply predictable from the linear optical response. It is rather influenced by intrinsic optical resonances as well as the emission characteristics which are strongly affected by the peculiar geometry of the devices. Since plasmonic nanostructures are always supported by a dielectric surrounding, its nonlinear contribution has to be taken into account as well. Finally, the nonlinear susceptibilities ($\chi^{(2)}, \chi^{(3)}, \dots$) of the involved materials are in most cases only vaguely known. For the case of second-harmonic generation, various theoretical approaches have been tested [8,12]. However, to successfully design plasmonic nanostructures that allow for efficient nonlinear conversion and which can be employed in nonlinear optics applications [13], a deeper understanding of the nonlinear processes is mandatory.

Here we show conclusively by means of third-harmonic generation (THG) spectroscopy and numerical simulations that the shape of the nonlinear spectra in hybrid plasmonic structures provides the answer to the eminent question of where the nonlinear response originates from, even if the *linear* spectra look similar. We further confirm our findings by a systematic variation of the constituent materials.

For the sake of discussing this problem in the framework of a particular example, we concentrate the investigation on metallic photonic crystals. Their linear optical response is well understood [14,15], rendering them an ideal plasmonic model system. The metallic photonic crystals we consider here consist of a 1D gold nanowire grating with a footprint of 100×100 μm^2 which is buried inside a dielectric slab waveguide on a quartz substrate (see Fig. 1, right inset). On the one hand, if the incident electric field polarization is perpendicular to the wires, localized plasmonic modes, so-called particle plasmon polaritons, are excited in the wires. On the other hand, the periodic arrangement of the wires allows coupling of the external illuminating field simultaneously to photonic waveguide modes in the dielectric slab. In the strong coupling regime the plasmonic and photonic modes hybridize to a waveguide plasmon polariton which is characterized by two extinction maxima (polaritonic eigenmodes) in the linear spectrum and an extinction dip in between. A sharp and deep dip in the extinction spectrum can be interpreted as a manifestation of plasmon-induced transparency [16,17]. Placing the metallic grating at the bottom of the waveguide
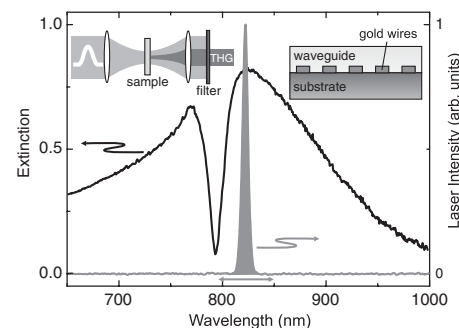
FIG. 1.   Linear extinction spectrum of the metallic photonic crystal structure (right inset, light incidence from the top) exhibiting a narrow extinction dip at 790 nm. The laser (gray area) can be tuned around the extinction dip from 750 to 900 nm. A schematic of the experimental setup is shown in the left inset.

will reduce the coupling of plasmonic and photonic modes due to a lower electric field overlap. Therefore, the polariton splitting of the two waveguide plasmon polariton modes decreases and one obtains extremely narrow features in the linear extinction spectrum [18]. We fabricate the samples by standard electron beam lithography and subsequent thermal evaporation of tungsten trioxide (WO_3) for the dielectric waveguide. Figure 1 shows the extinction $[-\ln(T), T:$ transmission] spectrum measured in a white light transmission setup. At 790 nm we observe a very narrow and pronounced dip in the broad extinction spectrum. From the strong extinction variations in a small spectral region, we can expect pronounced features also in the nonlinear spectrum.

In contrast to previous nonlinear experiments [19,20], we use rather narrow-band laser pulses from a Ti:sapphire oscillator ($t_{pulse} = 150$ fs, FWHM ≈ 7 nm). We slightly focus the light with an average power of 60 mW onto the sample to a spot size of 100 μm in order to avoid destruction (see Fig. 1, left inset). In the nonlinear regime we are restricted to THG due to the centrosymmetry of the grating. In a first experimental step we investigate a series of samples where the wire width varies from 70 to 80 and 90 nm, leading to a redshift of the particle plasmon resonance. The WO_3 waveguide thickness is 165 nm, the period of the grating is 530 nm, and the thickness of the gold wires is 15 nm. Figures 2(a)–2(c) show the linear extinction spectra of these samples. In all cases we observe the narrow extinction dip around 790 nm. Additionally, we plot linear spectra obtained from simulations using a scattering matrix formalism [21]. The numerical results agree nearly perfectly with the experiments. Figures 2(d)–2(f) show the experimentally obtained nonlinear THG spectra. To verify the exact position of the extinction dip, we first measure the extinction of the sample again for each

wavelength individually by using the laser. Finally, we measure the THG intensity obtained from the metallic photonic crystal as a function of the laser center wavelength. We normalize the THG signal of the sample to the THG signal obtained from the substrate including the waveguide slab but without the nanowires. With that procedure we assure that the THG intensity is not affected by experimental uncertainties which are due to the wavelength tuning of the laser. We convinced ourselves that only light at the threefold energy of the fundamental light was generated. Therefore, it is reasonable to measure the THG in a spectrally integrated fashion. In the nonlinear regime all three samples show similar behavior but with characteristic differences. We always observe a single spectral THG peak which appears at the spectral position of the extinction dip. A second THG peak occurs at the long-wavelength extinction maximum (waveguide plasmon polariton mode). While the first one maintains its spectral position for all three samples, the second peak is redshifted with increasing wire widths. This observation already indicates that the THG signal of the long-wavelength peak is related to the particle plasmon resonance in the metal wires. However, due to coupling and the polaritonic nature of the resonance, it is not *a priori* clear where the THG peak at the extinction dip stems from.

In order to gain more insight into the origin of the nonlinear response, we calculate the electric field distribution by using the scattering matrix algorithm. Figure 3(a) shows the electric field distribution for the wavelength of the extinction dip in Fig. 2(c). We observe a field enhancement in the waveguide and in the substrate while the field in the metal is low. Figure 3(b) shows the field for the extinction maximum at 832 nm. Now the field enhancement is mainly inside and in the vicinity of the metal. In the following we assume a local nonlinear polarization
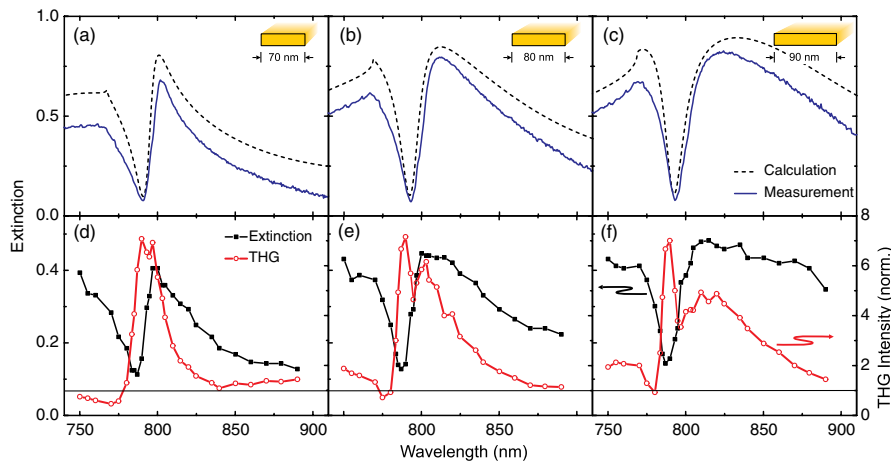
FIG. 2 (color online). (a)–(c) Extinction spectra of a sample series with a WO_3 waveguide (solid lines). The wire width is increased from (a) to (c); hence, the particle plasmon resonance is redshifted. The scattering matrix calculations show a good agreement with the experimental spectra (scattered lines). (d)–(f) Extinction measured stepwise with the 150 fs laser pulses (squares). The THG signal is normalized to the signal from substrate plus waveguide and is dominated by two peaks (circles).
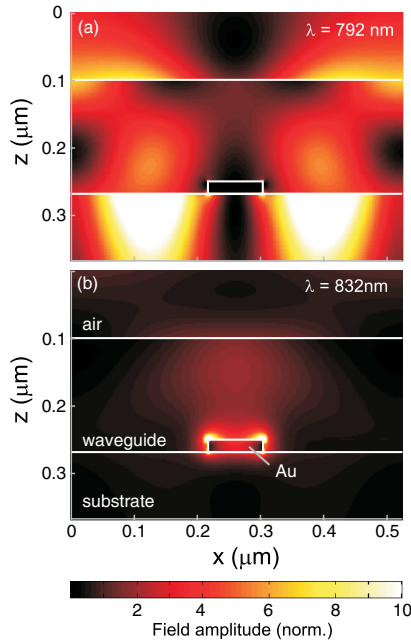
FIG. 3 (color online).   Amplitude of the electric field calculated for the unit cell of the structure. (a) At the wavelength of the extinction dip, the electric field is mainly concentrated inside the waveguide material and the substrate; no field is inside the metal. (b) At the extinction maximum, the electric field is located inside and in the vicinity of the metal. For optimum contrast, the linear color scale is limited to a value of 10.

$\mathbf{P}^{(\mathrm{NL})}(3\omega, \mathbf{r}) = \hat{\chi}^{(3)}(-3\omega; \omega, \omega, \omega, \mathbf{r})\vdots\mathbf{E}^3(\omega, \mathbf{r})$ which fully takes the dipolar bulk contributions of the involved materials into account. Obviously, the nonlinear polarization strongly depends on the actual field distribution inside the

nanostructure. Since the largest field enhancement is spectrally different inside the metal and in the dielectric, we expect that the two THG peaks are related to the actual constituent of the nanostructure. To confirm this assumption we perform numerical calculations that rely on an extended scattering matrix algorithm to determine THG in the forward direction [22]. By using this method, Maxwell's equations are solved rigorously within the framework of the undepleted pump approximation. The rather low absolute THG intensity observed in our experiments strongly justifies this assumption. We want to point out that no model assumptions with respect to the linear optical response enter the calculations. Applying this method, we fully take the tensorial character of the $\chi^{(3)}$ coefficients of all materials into account which are assumed to belong to a cubic isotropic crystallographic lattice. Then the tensor comprises only a single independent component. We neglect contributions from the quartz substrate because its THG signal is spectrally flat and rather weak.

We have calculated the THG spectrum for three different scenarios in order to investigate the individual contributions of the two materials. While keeping the linear properties of the structure identical, we adjust the ratios $\chi^{(3)}_{\mathrm{Au}}/\chi^{(3)}_{\mathrm{wg}}$ of the nonlinear coefficients. First, we investigate the two limiting cases when either $\chi^{(3)}_{\mathrm{wg}}$ or $\chi^{(3)}_{\mathrm{Au}}$ is set to zero. In Fig. 4(a), the nonlinearity of the dielectric waveguide material ($\chi^{(3)}_{\mathrm{wg}}$) is assumed to be zero. In this case, we obtain a THG spectrum whose shape largely resembles the linear extinction. At the extinction dip, where the electric field resides in the waveguide and is weak in the metal [compare Fig. 3(a)], we observe a reduced THG signal. On the contrary, if $\chi^{(3)}_{\mathrm{Au}}$ equals zero, the nonlinearity of the dielectric
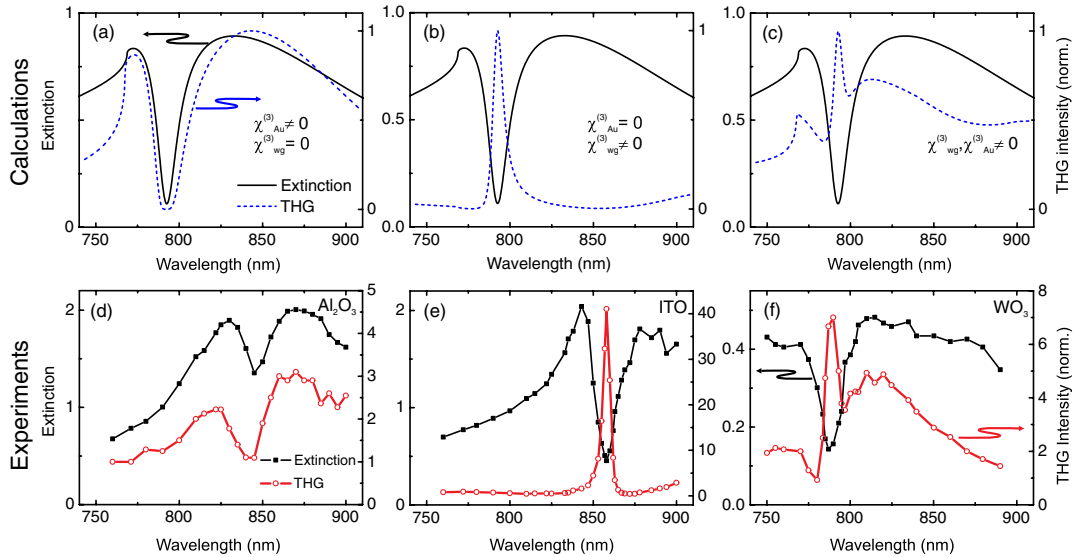
FIG. 4 (color online).   (a)–(c) Calculations for different $\chi^{(3)}_{\mathrm{Au}}/\chi^{(3)}_{\mathrm{wg}}$ ratios while keeping the linear optical properties constant. (d) Extinction and THG spectra of a sample with an Al_2O_3 waveguide. No THG peak is visible at the extinction dip; therefore, the metal contribution dominates. (e) In the case of indium tin oxide (ITO) as a waveguide material, its contribution dominates and leads to a strong THG peak at the extinction dip. (f) For the WO_3 waveguide we observe metal and dielectric contributions simultaneously.

waveguide is dominating [Fig. 4(b)]. In this case, the THG spectrum shows a pronounced peak which coincides with the extinction dip. Finally, by carefully adjusting the ratios of the nonlinear coefficients, we investigate the case where both materials contribute equally. Here we observe a combination of the two previous cases [Fig. 4(c)].

To experimentally confirm the influence of the materials on the nonlinear response, we fabricate another sample series where we change the dielectric material and therefore the magnitude of the nonlinearity of the waveguide. In Fig. 4(d), we show the linear and nonlinear spectrum of a sample with an Al_2O_3 waveguide which has a relatively small nonlinear coefficient ($\chi^{(3)} \approx 10^{-22} \frac{m^2}{V^2}$) that is on the order of the substrate [1]. For such a sample the THG spectrum follows exactly the extinction. This effect can be attributed to a dominating metal contribution to the nonlinear response. The waveguide material for Fig. 4(e) is indium tin oxide, which has on the contrary a rather large third-order coefficient ($\chi^{(3)} \approx 10^{-20} \frac{m^2}{V^2}$) [23]. In this case we obtain a strong THG peak at the extinction dip only because the dielectric contribution dominates. For direct comparison, Fig. 4(f) shows again the data for the WO_3 waveguide. Although we found no value for its $\chi^{(3)}$ in the literature, we infer that metal and dielectric nonlinearities contribute equally. In contrast to the simulations, the linear optical properties in the experiment change with the dielectric material as well. Therefore the measurements can be compared only qualitatively with respect to the spectral axis.

In conclusion, we used THG spectroscopy to demonstrate that the nonlinear optical response of a hybrid plasmonic nanostructure is strongly dependent on the constituent materials. By using plasmonic nanowires and varying the materials for the dielectric waveguide slab beneath, as well as the ratio of its nonlinearities $\chi_{Au}^{(3)}/\chi_{wg}^{(3)}$, the shape of the THG spectrum can change significantly even if the linear spectra are very similar. From electric field distribution simulations we find that the dominant contributing material to the nonlinear response can be predicted from the shape of the nonlinear spectrum. In the future, quantitative comparisons certainly will help to determine *ab initio* the nonlinear susceptibilities of plasmonic nanostructures and plasmon-induced transparency systems [17] and will allow for the efficient design of future nonlinear integrated devices.

[1] R. W. Boyd, *Nonlinear Optics* (Elsevier, New York, 2008), 3rd ed.

[2] C. K. Chen, A. R. B. de Castro, and Y. R. Shen, Phys. Rev. Lett. **46**, 145 (1981).

[3] C. K. Chen, T. F. Heinz, D. Ricard, and Y. R. Shen, Phys. Rev. B **27**, 1965 (1983).

[4] M. Lippitz, M. A. van Dijk, and M. Orrit, Nano Lett. **5**, 799 (2005).

[5] B. K. Canfield, H. Husu, J. Laukkanen, B. Bai, M. Kuittinen, J. Turunen, and M. Kauranen, Nano Lett. **7**, 1251 (2007).

[6] S. Kujala, B. K. Canfield, M. Kauranen, Y. Svirko, and J. Turunen, Phys. Rev. Lett. **98**, 167403 (2007).

[7] T. Hanke, G. Krauss, D. Trautlein, B. Wild, R. Bratschitsch, and A. Leitenstorfer, Phys. Rev. Lett. **103**, 257404 (2009).

[8] F. X. Wang, F. J. Rodriguez, W. M. Albers, R. Ahorinta, J. E. Sipe, and M. Kauranen, Phys. Rev. B **80**, 233402 (2009).

[9] A. Anderson, K. S. Deryckx, X. J. G. Xu, G. Steinmeyer, and M. B. Raschke, Nano Lett. **10**, 2519 (2010).

[10] M. W. Klein, C. Enkrich, M. Wegener, and S. Linden, Science **313**, 502 (2006).

[11] F. B. P. Niesler, N. Feth, S. Linden, J. Niegemann, J. Gieseler, K. Busch, and M. Wegener, Opt. Lett. **34**, 1997 (2009).

[12] Y. Zeng, W. Hoyer, J. J. Liu, S. W. Koch, and J. V. Moloney, Phys. Rev. B **79**, 235109 (2009).

[13] J. Renger, R. Quidant, N. van Hulst, and L. Novotny, Phys. Rev. Lett. **104**, 046803 (2010).

[14] S. Linden, J. Kuhl, and H. Giessen, Phys. Rev. Lett. **86**, 4688 (2001).

[15] A. Christ, T. Zentgraf, J. Kuhl, S. G. Tikhodeev, N. A. Gippius, and H. Giessen, Phys. Rev. B **70**, 125113 (2004).

[16] V. Yannopapas, E. Paspalakis, and N. V. Vitanov, Phys. Rev. B **80**, 035104 (2009).

[17] B. Luk'yanchuk, N. I. Zheludev, S. A. Maier, N. J. Halas, P. Nordlander, H. Giessen, and C. T. Chong, Nature Mater. **9**, 707 (2010).

[18] T. Zentgraf, S. Zhang, R. F. Oulton, and X. Zhang, Phys. Rev. B **80**, 195415 (2009).

[19] T. Zentgraf, A. Christ, J. Kuhl, and H. Giessen, Phys. Rev. Lett. **93**, 243901 (2004).

[20] T. Utikal, M. I. Stockman, A. P. Heberle, M. Lippitz, and H. Giessen, Phys. Rev. Lett. **104**, 113903 (2010).

[21] S. G. Tikhodeev, A. L. Yablonskii, E. A. Muljarov, N. A. Gippius, and T. Ishihara, Phys. Rev. B **66**, 045102 (2002).

[22] T. Paul, C. Rockstuhl, and F. Lederer, J. Opt. Soc. Am. B **27**, 1118 (2010).

[23] N. Ueda, H. Kawazoe, Y. Watanabe, M. Takata, M. Yamane, and K. Kubodera, Appl. Phys. Lett. **59**, 502 (1991).